



Integrated Single Cell Analysis Reveals An Atlas of Tumor Associated Macrophages in Hepatocellular Carcinoma

Xinqiang Li^{1,2}, Ruixia Li³, Xiaolong Miao^{1,2}, Xin Zhou^{1,2}, Bin Wu^{1,2}, Junning Cao^{1,2}, Chengyu Wang^{1,2}, Shipeng Li^{4,5} and Jinzhen Cai^{1,2,5}

Received 25 November 2023; accepted 12 April 2024

Abstract—Hepatocellular carcinoma (HCC), one of the most prevalent cancers globally, is closely associated with tumor-associated macrophages (TAMs), including monocyte-derived macrophages and liver-resident Kupffer cells. Understanding TAM heterogeneity at the cellular level is crucial for developing effective HCC prevention and treatment strategies. In this study, we conducted an integrated single-cell analysis of four cohorts (GSE140228, GSE125449, GSE149614 and GSE156625) to elucidate the TAM landscape in HCC. We identified 284 gene markers, termed Panmyeloid markers, that characterize myeloid cells within this context. Our analysis distinguished six clusters of monocyte-derived macrophages (Macro1-Macro6) and four clusters of Kupffer cells (Kupffer1-Kupffer4). Notably, CXCL10+ macrophages and MT1G+ Kupffer cells, predominantly located within tumor tissues, exhibited distinct functional characteristics relevant to HCC. We also explored cellular communication between TAMs and T cells, uncovering potential signaling pathways such as the CXCL10/CXCL11-CXCR3 and CXCL12-CXCR4 networks. These findings enhance our understanding of TAMs in HCC and open new avenues for targeted therapeutic interventions.

KEY WORDS: Tumor associated macrophages; Hepatocellular carcinoma; Single-cell RNA sequencing; CXCL10+ Macrophages; MT1G+ Kupffer cells

Xinqiang Li and Ruixia Li contributed equally to this work.

¹Organ Transplantation Center, Affiliated Hospital of Qingdao University, Qingdao, China

²Institute of Organ Donation and Transplantation, Medical College of Qingdao University, Qingdao, China

³Department of Pulmonary and Critical Care Medicine, Second Affiliated Hospital of Harbin Medical University, Harbin, China

⁴Department of Hepatopancreaticobiliary Surgery, Henan Provincial People's Hospital, Zhengzhou University, Zhengzhou, China

⁵To whom correspondence should be addressed at Organ Transplantation Center, Affiliated Hospital of Qingdao University, Qingdao, China and Department of Hepatopancreaticobiliary Surgery, Henan Provincial People's Hospital, Zhengzhou University, Zhengzhou, China. Email: caijinzhen@qdu.edu.cn; shipengli2010@163.com

INTRODUCTION

Hepatocellular carcinoma (HCC) stands as a major global health challenge, representing one of the most common and aggressive cancers worldwide with a continually rising incidence and poor prognosis. The complexity of HCC pathogenesis, coupled with its late diagnosis and limited therapeutic options, underscores the urgent need for deeper insights into its underlying mechanisms [1, 2]. Recent advances in understanding HCC have highlighted the pivotal role of the tumor immune microenvironment, particularly focusing on the function and influence of tumor-associated macrophages (TAMs). TAMs, comprising

monocyte-derived macrophages and liver-specific Kupffer cells, are increasingly recognized for their significant contributions to HCC progression and metastasis. Their dynamic interactions within the tumor microenvironment influence various aspects of HCC, from tumor initiation to metastatic spread [3–5].

Despite this recognition, a comprehensive understanding of TAM heterogeneity and function at the cellular level in HCC remains elusive. Previous research has provided valuable insights yet often lacked a holistic view, focusing on specific cell clusters or a limited set of gene markers [6]. This has hindered the construction of a detailed landscape of TAMs' heterogeneity and their multifaceted roles in HCC. The advent of single-cell RNA sequencing (scRNA-seq) technology offers an unprecedented opportunity to unravel the complex cellular composition of human tissues, including HCC. By enabling a high-resolution view of individual cells, scRNA-seq has been instrumental in delineating the diverse immune phenotypes and intricate cell–cell interactions within HCC [7–10]. Pioneering studies have shed light on the distinct subtypes of infiltrating lymphocytes, the inflammatory states of myeloid cells, and the nuanced interplay between various immune cells within the HCC microenvironment [11, 12]. Consequently, further research is imperative to comprehensively delineate both the patterns and the potential roles of TAMs in HCC, which could be crucial for advancing our understanding and treatment of this disease.

In this study, we leverage the power of scRNA-seq to conduct an integrated analysis of four comprehensive cohorts, encompassing 70 HCC samples. Our aim is to provide a detailed characterization of the TAM landscape in HCC. By offering a comprehensive view of TAM heterogeneity and interaction networks in HCC, this study aims to fill a critical gap in our understanding and pave the way for novel therapeutic approaches targeting the tumor microenvironment.

RESULTS

Integration of Single Cell Cohorts in Human HCC

We integrated single cell RNA sequencing datasets from human HCC samples, as detailed in Table S1. For data integration, we employed the Mutual Nearest Neighbors (MNN) method [13] (Fig. 1a), chosen for its efficacy in minimizing batch effects across datasets. To further reduce potential batch effects, we carefully controlled for variables

such as sequencing techniques, disease types, and species. All datasets were derived using 10X Genomics technology, specifically employing the Chromium Single Cell 3' Library, Gel Bead & Multiplex Kit, and Chip Kit. Each sample analyzed was histologically diagnosed as HCC.

Following the integration and subsequent clustering process, we identified cell type annotations using canonical markers (Table S2). This process yielded a total of 32 distinct clusters, encompassing 135,900 cells, across 70 samples (Fig. 1b). The distribution of these clusters across various tissue samples is visually represented in Fig. S1A, with specific tissue locations detailed in Fig. S1B. Hepatocyte and cholangiocyte markers were used to distinguish epithelial clusters (Fig. 1b, Fig. S1C). Among the clusters, a noteworthy finding was the identification of 23,010 myeloid cells. These cells were predominantly categorized into clusters 3, 5, 16, 19, 21, 22, 25, and 26 (Fig. 1b). This significant subset of cells offers potential insights into the myeloid cell landscape and their roles in the pathology of HCC.

Panmyeloid Marker Profiling by Lineage and Tissue in Hepatocellular Carcinoma

Following our detailed annotation of the cell landscapes in human HCC (Fig. 2a), we re-analyzed differentially expressed genes within various cell lineages. Utilizing canonical myeloid markers—CD68, CD14, and CD163—we isolated myeloid cells and identified 284 gene markers. These markers, termed 'Panmyeloid markers,' form a unique gene list representative of myeloid cells in HCC (Table S3). Notably, these markers showed significant expression in TAMs and dendritic cells (DCs), compared to other cell types (Fig. 2b).

Panmyeloid markers encompass genes encoding proteins essential for diverse myeloid cell functions, such as migration (e.g., AIF1, CXCL8, IL1B, CD74), differentiation (C1QC, CCL3, TYROBP, FCER1G), cytokine production (CD74, CD36, NR4A3), and homeostasis (FCER1G, MAFB, HMOX1, SPI1) [14, 15]. Additionally, these markers play crucial roles in myeloid-leucocyte interactions, with genes involved in leucocyte chemotaxis, migration, and degranulation (CST3, CST8, LYZ, CD68) [16, 17]. Furthermore, some markers participate in Toll-like receptor binding (S100A8, S100A9, LY96) and lipopeptide binding (CD1C, CD1E) [18, 19].

We identified two primary myeloid cell groups in HCC: TAMs and DCs. TAMs, known for their production of pro-inflammatory or pro-tumorigenic cytokines,

Integrated single cell analysis reveals an atlas of tumor associated...

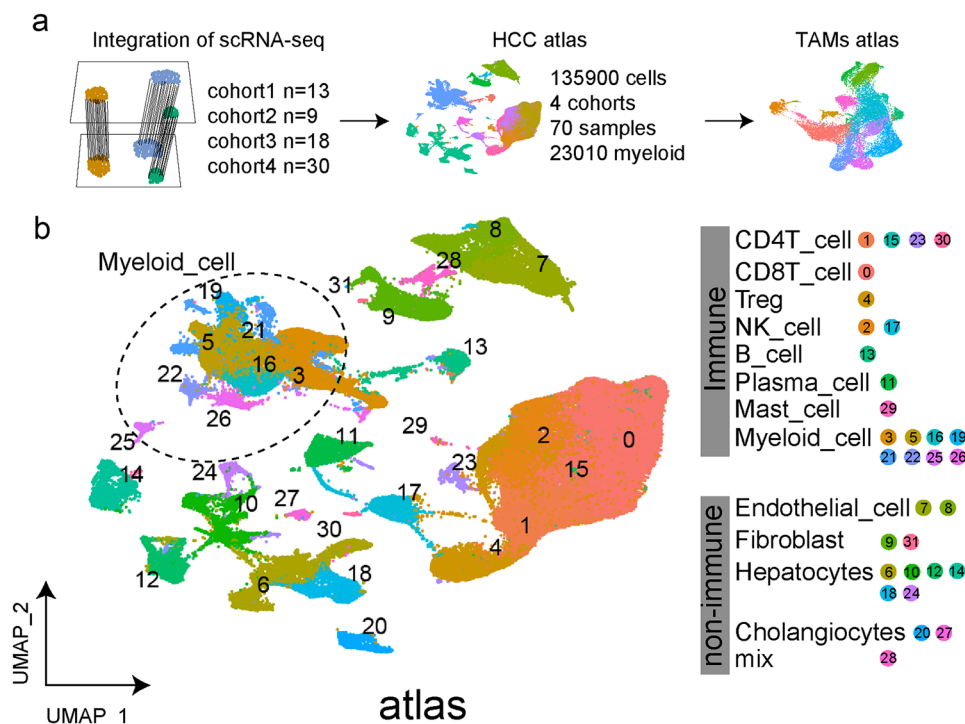


Fig. 1 Overview of the study design and integrated dataset. **a** Overview of the study design. Single-cell RNA sequencing of 4 cohorts (GSE140228, N=13; GSE125449, N=9; GSE149614, N=18 and GSE156625, N=15) were integrated to form the hepatocellular atlas. **b** UMAP representation of the hepatocellular carcinoma as obtained from 135,900 cells of 70 tumor samples using dotplot. Each dot represents a single cell.

display characteristics that can be either anti-tumor [20] or pro-tumor [21]. Panmyeloid markers in TAMs include genes associated with tumorigenesis (VEGFA, TGFB1, PDGFA) and inflammation (FCGR3A, IL12, TNF). DCs predominantly function in antigen processing and presentation, with related genes (HLA-DRA, FCER1G, FGL2, CTSD) also present in Panmyeloid markers [22–24]. To rigorously validate the effectiveness of Panmyeloid markers, we conducted a detailed myeloid score analysis leveraging a comprehensive set of 284 gene markers. This analysis revealed that, within the spectrum of myeloid cell groups, Kupffer cells registered notably higher scores in comparison to both macrophages and DCs (Fig. 2c). When broadening the comparison to encompass other immune cells, including B cells, NK cells, and T cells, it became evident that all myeloid cell groups exhibited significantly elevated myeloid scores (Fig. 2c, Fig. S2). These findings underscore the utility of Panmyeloid markers in distinguishing between myeloid cells and other types of immune cells with a high degree of precision.

Moreover, we identified specific markers, termed ‘location markers,’ differentially expressed between tumor and adjacent tissues (Table S3). The top ten markers with up-regulation (based on average logFC) were SPP1, RNASE1, APOC1, APOA2, MMP12, APOE, MMP9, NUPR1, CSTB, and FABP5. Conversely, the top ten markers with down-regulation included THBS1, CXCL12, S100A9, IGHA1, S100A8, CFP, LYVE1, CETP, PLAC8, and MARCO (Table S3). Significantly, 67 genes found at the intersection of Panmyeloid and location markers showed high expression in HCC tumor sites (Table S3), and 44 were down-regulated (Table S3).

Identification of Monocyte-Derived Macrophages and Kupffer Cells in Hepatocellular Carcinoma

In our detailed analysis of TAMs in HCC, we re-clustered the myeloid cell population (23,010 cells) and performed an in-depth annotation (Table S4). This analysis distinguished 6 clusters of monocyte-derived

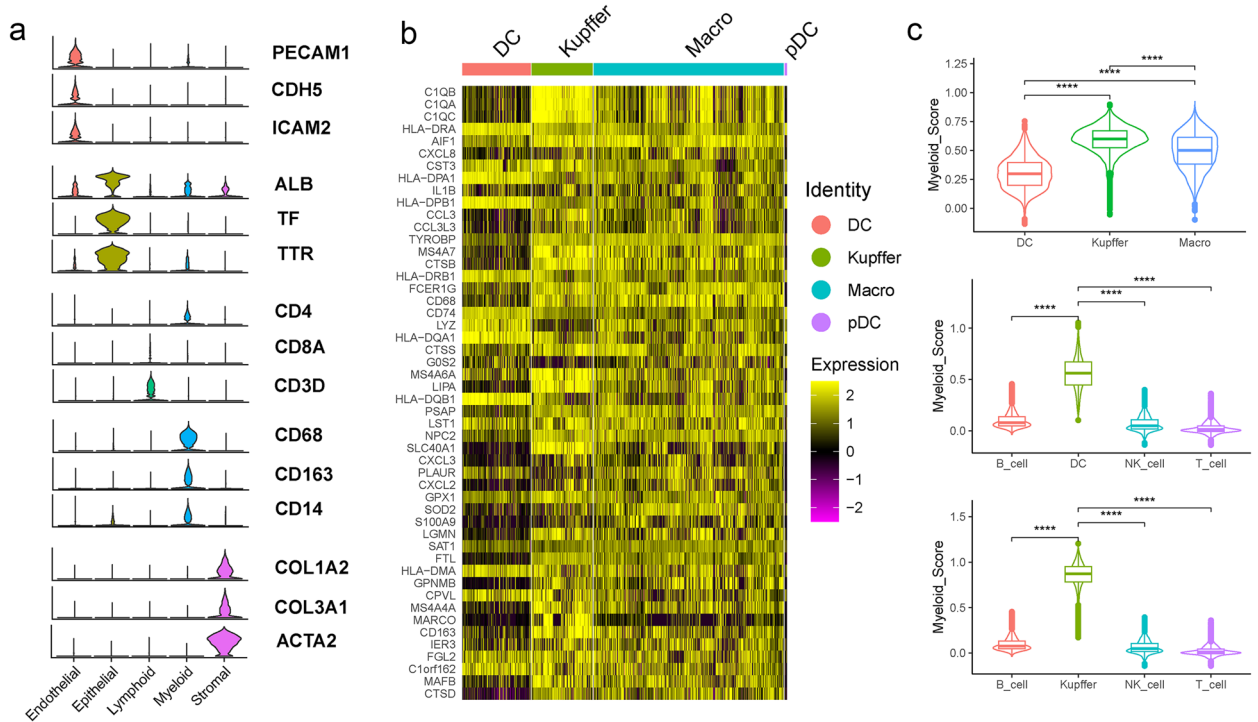


Fig. 2 Visualization of Panmyeloid markers for myeloid cells of human HCC by single-cell RNA sequencing. **a** Violin plots showing the annotation of cell types according to canonical markers: PECAM1, CDH5 and ICAM2 for endothelial cells; ALB, TF and TTR for epithelial cells; CD4, CD8A and CD3D for lymphoid cells; CD68, CD163 and CD14 for myeloid cells; COL1A2, CDL3A1 and ACTA2 for stromal cells. **b** Heatmap showing the top 50 genes of Panmyeloid markers. DC, pDC, Kupffer and Macrophages were all highly expressed within the genes listed above. **c** Violin plots showing the myeloid scores among myeloid cell groups and other immune cells (**** means $p < 0.0001$).

macrophages (Macro1-Macro6) and 4 clusters of Kupffer cells (Kupffer1-Kupffer4) from the 5 clusters of dendritic cells (DCs) (Fig. 3a-d).

Utilizing canonical markers, we classified the monocyte-derived macrophages into three broad categories: 1) pro-tumorigenic (10,152 cells in Macro 1, 2, 4, and 6), 2) pro-inflammatory (1,705 cells in Macro 5), and 3) myeloid-derived suppressor cells (MDSCs, 2,366 cells in Macro 3) (Table S4, Fig. 4A). The pro-tumorigenic macrophages, exhibiting an M2 polarized phenotype, were characterized by high expression of factors including transforming growth factor β 1 (TGFB1) [25], vascular endothelial growth factor A (VEGFA) [26, 27], platelet-derived growth factor (PDGFA and PDGFB) [28], IL6 [29], IL1B [30], CD163, CCL2 [31], proliferative factors (CD206 and MKI67), and tumor necrosis factor (TNF) [32]. These factors are known to contribute to tumor growth and proliferation (Table S4).

In contrast, the pro-inflammatory macrophages (M1 polarized phenotype) demonstrated elevated levels of immunostimulatory pro-inflammatory factors such as FCGR3A, IL12, and TNF (Table S4). MDSCs were characterized by high expression of immunosuppressive factors, including THBS1, FCN1, VCAN, and CD33 [33] (Table S4).

Further dissection of the pro-tumorigenic macrophages revealed four distinct subpopulations, which will be described in subsequent sections.

In the resident liver macrophage population, we identified two major subsets of Kupffer cells: MARCO+ (3,201 cells in Kupffer1 and 2) and MARCO- (1,173 cells in Kupffer 3 and 4), differentiated using specific markers (Fig. 5a). MARCO+ Kupffer cells were marked by high expression of MARCO, TIMD4, and activated cytokines including CCL2, CCL5, interleukin 1 β (IL-1 β), and TNF. Conversely, MARCO- Kupffer

Integrated single cell analysis reveals an atlas of tumor associated...

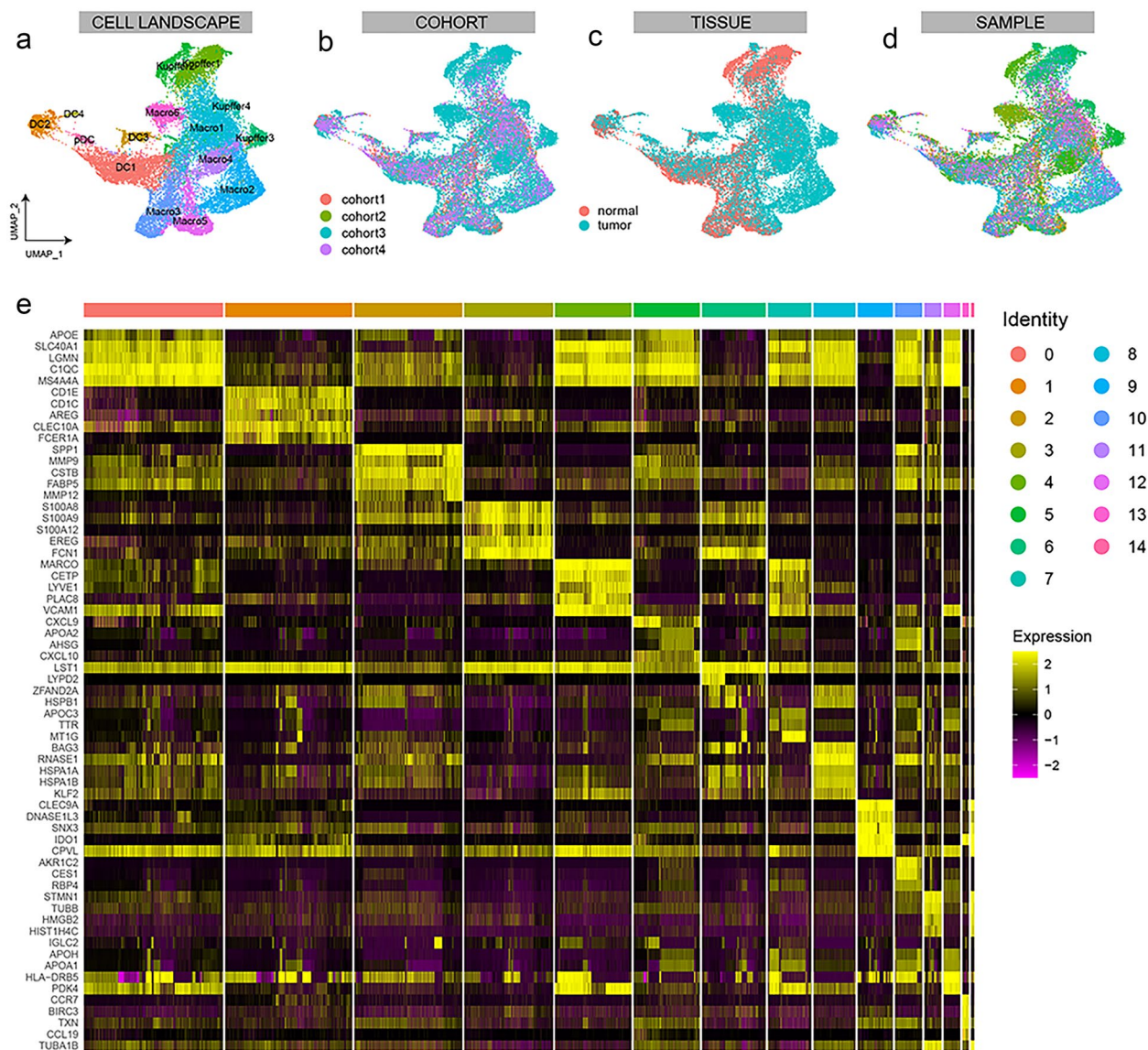


Fig. 3 Visualization of myeloid cells of human HCC by single-cell RNA sequencing. **a** UMAP of 23,010 myeloid cells from 70 samples showing the landscape of myeloid cells for human HCC consisting of 5 clusters for DCs, 6 clusters for monocyte-derived macrophages and 4 clusters for Kupffer cells. **b** UMAP of myeloid cells by 4 cohorts. **c** UMAP of myeloid cells by location in tumor and normal tissues. **d** UMAP of myeloid cells within the 70 samples. **e** Heatmap showing the top 5 differentially expressed genes of each cluster.

cells predominantly expressed CD5L and VCAM1. Notably, all Kupffer cell types exhibited elevated levels of macrophage mannose receptor 1-like protein (MRC1 or CD206), a type I membrane receptor crucial for the endocytosis of glycoproteins by macrophages (Table S4).

Distinct Features of Spatially Heterogeneous Monocyte-Derived Macrophages in Hepatocellular Carcinoma

We conducted an in-depth assessment of the spatial distribution and distinct characteristics of three

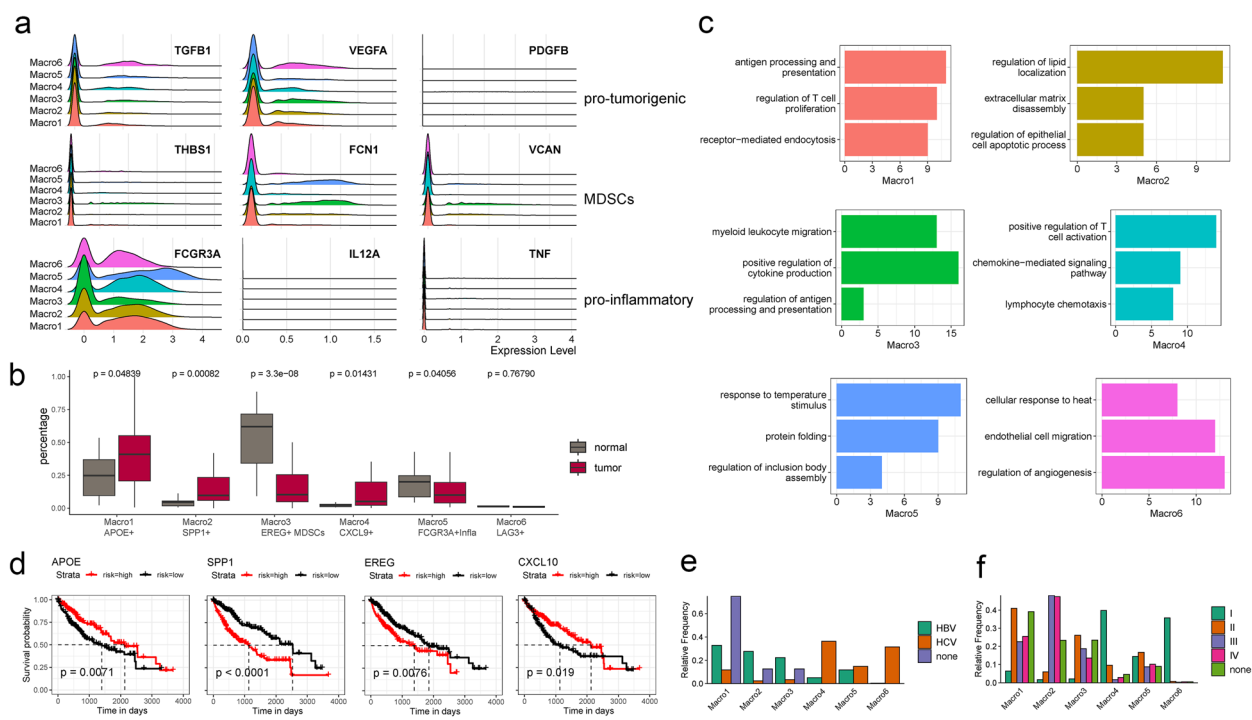


Fig. 4 Accessing monocyte-derived macrophage heterogeneity in human HCC. **a** RidgePlots showing expressions of pro-tumorigenic (TGFB β 1, VEGF α and PDGF β) and pro-inflammatory (FCGR3A, IL12A and TNF) macrophages and MDSCs (THBS1, FCN1 and VCAN) of monocyte-derived macrophages. **b** Fractions of monocyte-derived macrophage subpopulations in normal and tumor samples. **c** Bar plots showing the GO functional analysis for DEGs of each macrophage group. **d** KM analysis showing each marker gene of subpopulations for survival of TCGA. **e** Fractions of monocyte-derived macrophage subpopulations based on the etiology of HCC. **f** Fractions of monocyte-derived macrophage subpopulations based on the tumor stage of HCC.

broad categories of monocyte-derived macrophages in HCC. Our findings revealed a predominance of pro-tumorigenic macrophages within tumor tissues, while pro-inflammatory macrophages and myeloid-derived suppressor cells (MDSCs) were more prevalent in tumor-adjacent tissues (Fig. 4b).

We conducted macrophage's identification using specific gene expression and functional enrichment analysis. APOE + Macro1 cells were characterized by gene expressions primarily involved in antigen processing and presentation via MHC class II molecules (e.g., HLA-DMB, HLA-DMA, HLA-DPA1, HLA-DRB1) and in regulating endocytosis (e.g., APOE, DAB2, TREM2, CD14) and T cell proliferation (Fig. 4c, Table S5). SPP1 + Macro2 cells exhibited high levels of secreted phosphoprotein 1 (SPP1) expression, a key component of the epithelial-mesenchymal transition (EMT) pathway, and participated in extracellular matrix receptor communication [34]. Besides SPP1, Macro2

also expressed genes related to lipid localization (e.g., ANXA2, APOC1, CD36) and extracellular matrix (ECM) organization (e.g., MMP9, MMP12, CTSL) (Fig. 4c, Table S5).

CXCL10 + Macro4 demonstrated a diverse range of genes within the chemokine family (e.g., CXCL9, CXCL10, CXCL11, CXCL13), associated with positive responses to immune checkpoint blockade (ICB) in antitumor immunity [35]. Notably, immune checkpoints PD-1, PD-L1 (CD274), and CTLA-4 were all highly expressed in CXCL10 + Macro4. Functional enrichment analysis suggested the association with T cell proliferation, chemokine-mediated signal and lymphocyte chemotaxis (Fig. 4c, Table S5). Macro6, another subtype of pro-tumorigenic macrophages, exhibited the highest expression levels of Bcl2-associated athanogene 3 (LAG3), a co-chaperone of the heat-shock protein (HSP) 70, along with several other HSP family genes (e.g., HSPA1A, HSPA1B, HSPB1, HSPH1), associated with

Integrated single cell analysis reveals an atlas of tumor associated...

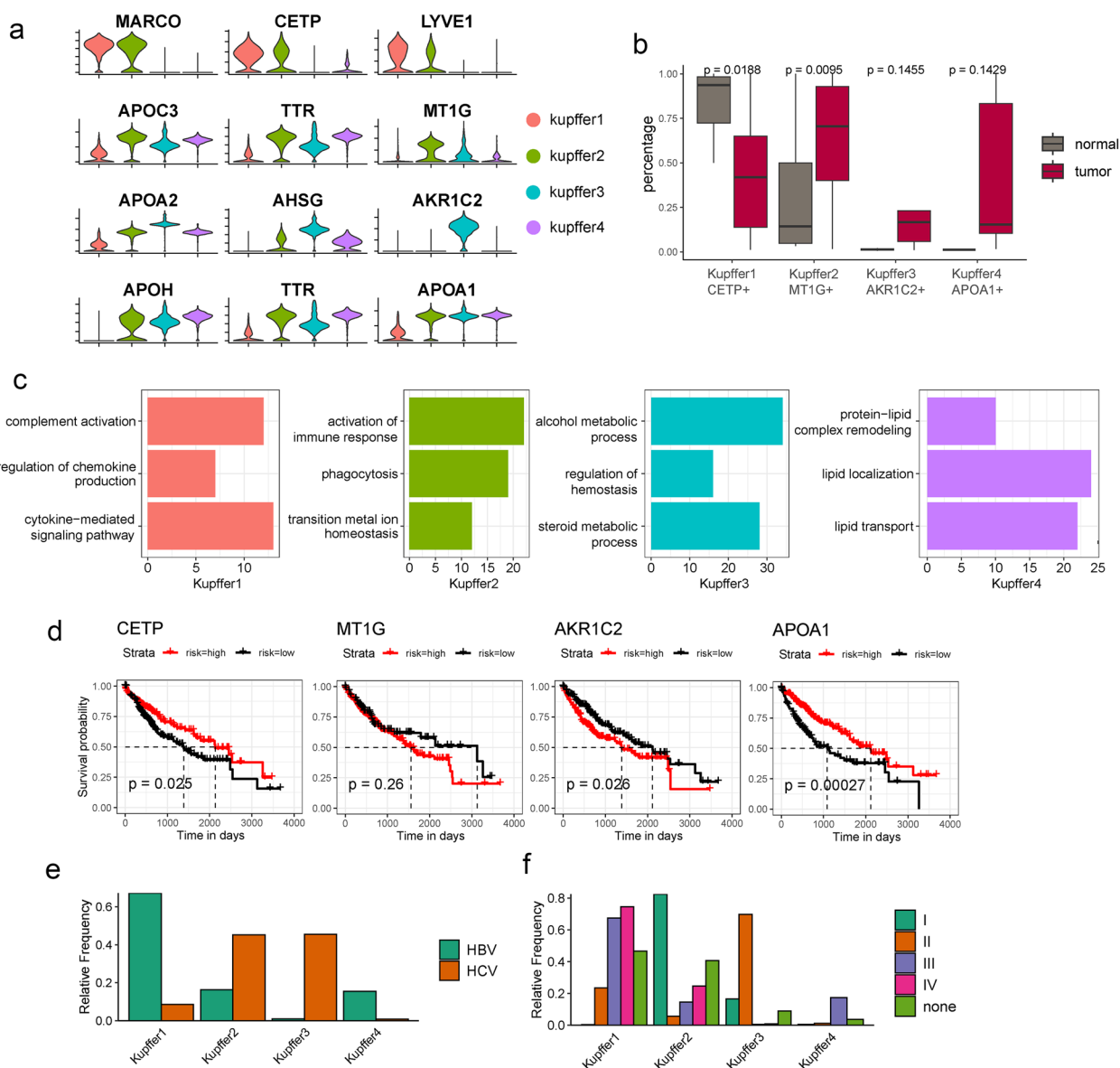


Fig. 5 Accessing Kupffer cell heterogeneity in human HCC. **a** Violin Plots showing the expression of markers of Kupffer subgroups. **b** Fractions of Kupffer cell subpopulations in normal and tumor samples. **c** Bar plots showing the GO functional analysis for DEGs of each kupffer group. **d** KM analysis showing each marker gene of subpopulations for survival of TCGA. **e** Fractions of Kupffer cell subpopulations based on the etiology of HCC. **f** Fractions of Kupffer cell subpopulations based on the tumor stage of HCC.

cellular response to heat and regulation of angiogenesis (Fig. 4c, Table S5).

EREG + MDSCs (Macro3) were distinguished by high expression levels of THBS1, FCN1, VCAN, and EREG, indicating a heterogeneous population of immature myeloid cells with impaired antigen-presenting

functions [15, 36]. The top markers of MDSCs, including S100A8, S100A9, and S100A12, were involved in the nuclear factor-kappaB (NF-kappaB) signaling pathway, which plays a role in inflammation-induced HCC progression [37] and the formation of a neutrophil chemokine network with CXCL2 [38] (Fig. 4c, Table S5). Epiregulin

(*EREG*), the fourth most highly expressed MDSC marker, encodes a secreted peptide hormone of the epidermal growth factor (*EGF*) family, promoting HCC progression. The knockdown of *EREG* has been shown to suppress the growth of human hepatoma cells [39], suggesting that *EREG*+MDSCs could be a potential target for HCC therapy. The top ten markers of pro-inflammatory macrophages (*FCGR3A*+*Macro5*) include genes such as *FCN1*, *LST1*, *COTL1*, *S100A6*, *IFITM3*, *LYPD2*, *BCL2A1*, *TIMP1*, *LILRB2*, and *HSP90AA1*. Functional enrichment analysis showed *FCGR3A*+*Macro5* were involved of response to temperature, protein folding and regulation of inclusion body assembly (Fig. 4c, Table S5).

Our survival analysis of representative genes within each macrophage cluster revealed significant prognostic implications for HCC. High levels of *APOE* (*Macro1*) and *CXCL10* (*Macro4*) expression were associated with enhanced patient survival, while high levels of *SPP1* (*Macro2*) and *EREG* (*Macro3*) correlated with poorer outcomes (Fig. 4d, Fig. S3). Further investigations into the differences among TAM classes relative to the underlying liver disease and presumed HCC etiology (Fig. 4e) indicated that *Macro1* showed a non-viral aetiology, whereas *Macro2* and *Macro3* were associated with hepatitis B virus (HBV) infection. In contrast, *Macro4* and *Macro6* were more relevant to hepatitis C virus (HCV) infection. Additionally, our findings suggested that *Macro4* and *Macro6* were prevalent in early-stage HCC, whereas *Macro1* and *Macro2* were more common in advanced stages of the disease (Fig. 4f).

scRNAseq Characterization of Liver-Resident Macrophages

Kupffer cells, the resident macrophages of the liver, are known for their self-renewing and non-migratory nature, playing a pivotal role in maintaining liver homeostasis [40]. Utilizing known markers, we identified two distinct subpopulations of Kupffer cells: *MARCO*+ (3,201 cells in *Kupffer1* and *Kupffer2*) and *MARCO*- (1,173 cells in *Kupffer3* and *Kupffer4*) (Fig. 5a).

MARCO+ *Kupffer1* cells, predominantly found in tumor-adjacent tissues (Fig. 5b), exhibited gene expressions associated with complement activation (e.g., *CFD*, *CFP*, *C1QA*, *C1QB*, *C2*), immune responses, and chemokine/cytokine metabolic processes (e.g., *HMOX1*, *EGR1*, *IL18*, *TNF*, *IL6*) (Fig. 5c, Table S6). This profile is indicative of classical Kupffer cell functions.

Additionally, the cholesteryl ester transfer protein (*CETP*) in these cells plays an immunological gatekeeping role by enhancing high-density lipoprotein (HDL) production, predominantly from Kupffer cells [41, 42]. The second group, *MT1G*+*Kupffer2* cells, more prevalent in tumor tissues (Fig. 5b), express *Metallothionein 1G* (*MT1G*), known as a suppressor of HCC tumor growth [43]. Functional analysis showed that *MT1G*+*Kupffer2* was associated with activation of immune response, phagocytosis and transition metal ion homeostasis (Fig. 5c, Table S6).

Conversely, *MARCO*- Kupffer cells, specifically *Kupffer3*, demonstrated an increased presence in tumor tissues. The top five markers in these cells included *APOA2*, *AHSG*, *AKR1C2*, *CES1*, and *RBP4*. Notably, *AKR1C2*, minimally expressed in other cells, is linked to HCC metastasis when combined with *AEG-1* [44, 45]. Functional analysis showed the correlation with alcohol metabolic process, regulation of hemostasis and steroid metabolic process (Fig. 5c, Table S6). *Kupffer4*, while sharing gene expressions with other Kupffer cells, also expresses genes (*APOA1*, *APOA3*, *FABP1*, *SLC27A5*, *PLTP*) that potentially suppress HCC metastasis via the *PPAR* signaling pathway, which was associated with protein-lipid complex remodeling, lipid localization and lipid transport (Fig. 5c, Table S6).

We conducted a survival analysis of representative genes from each Kupffer cell cluster, which indicated that high expression of *CETP* and *APOA1* was significantly associated with good outcome while highly expressed *AKR1C2* was significantly linked with poor outcome (Fig. 5d). Further analysis elucidated the etiology of each Kupffer cell cluster, revealing that *Kupffer1* and *Kupffer4* were associated with hepatitis B virus (HBV) infection, whereas *Kupffer2* and *Kupffer3* showed a predisposition to hepatitis C virus (HCV) infection (Fig. 5e). Regarding tumor stages, *Kupffer2* and *Kupffer3* were identified in early-stage HCC, while *Kupffer1* and *Kupffer4* were found in advanced stages (Fig. 5f).

Panmyeloid markers also distinguish TAMs among ICC samples.

The specificity of these findings to HCC was initially unclear, as control lesions had not been analyzed. To address this, we examined an intrahepatic cholangiocarcinoma (ICC) cohort containing 8 samples. Post cell filtration and clustering, we obtained 32,172 high-quality cells (Fig. 6a), with cell type annotations determined using canonical markers, including cholangiocyte, hepatocyte, malignant cell, endothelial cell, fibroblast, myeloid cell, T cell and B cell (Table S2;

Fig. 6b, c and Fig. S4). A total of 21 clusters, including 5,161 myeloid cells, were identified across the 8 samples. After re-clustering all myeloid cells, we annotated DCs, Kupffer cells, and monocyte-derived macrophages (Fig. 6d). We conducted gene expression analysis for marker genes from HCC macrophages and found that macro6 from ICC showed high expression of APOE, CXCL9, FCGR3A and LAG3, macro1 highly expressed SPP1 and macro4 highly expressed EREG (Fig. 6e). To further assess the validity of Panmyeloid markers in distinguishing cellular profiles within ICC, we embarked on a myeloid score analysis. This investigation revealed that, in alignment with observations in HCC, Kupffer cells in ICC manifested higher scores when compared to macrophages and DCs. Moreover, across the spectrum of immune cells analyzed, including B cells and T cells,

all myeloid cell groups in ICC consistently demonstrated significantly elevated myeloid scores (Fig. 6f). These findings corroborate the effectiveness of Panmyeloid markers in distinguishing myeloid cells from other immune cell types within the ICC environment, thus highlighting their potential applicability in furthering our understanding of hepatic diseases.

Cellular Communication Among TAMs and Other Cell Populations in Hepatocellular Carcinoma

The role of TAMs in HCC development and metastasis is significantly influenced by their interactions with other cell populations within tumor tissues. To explore

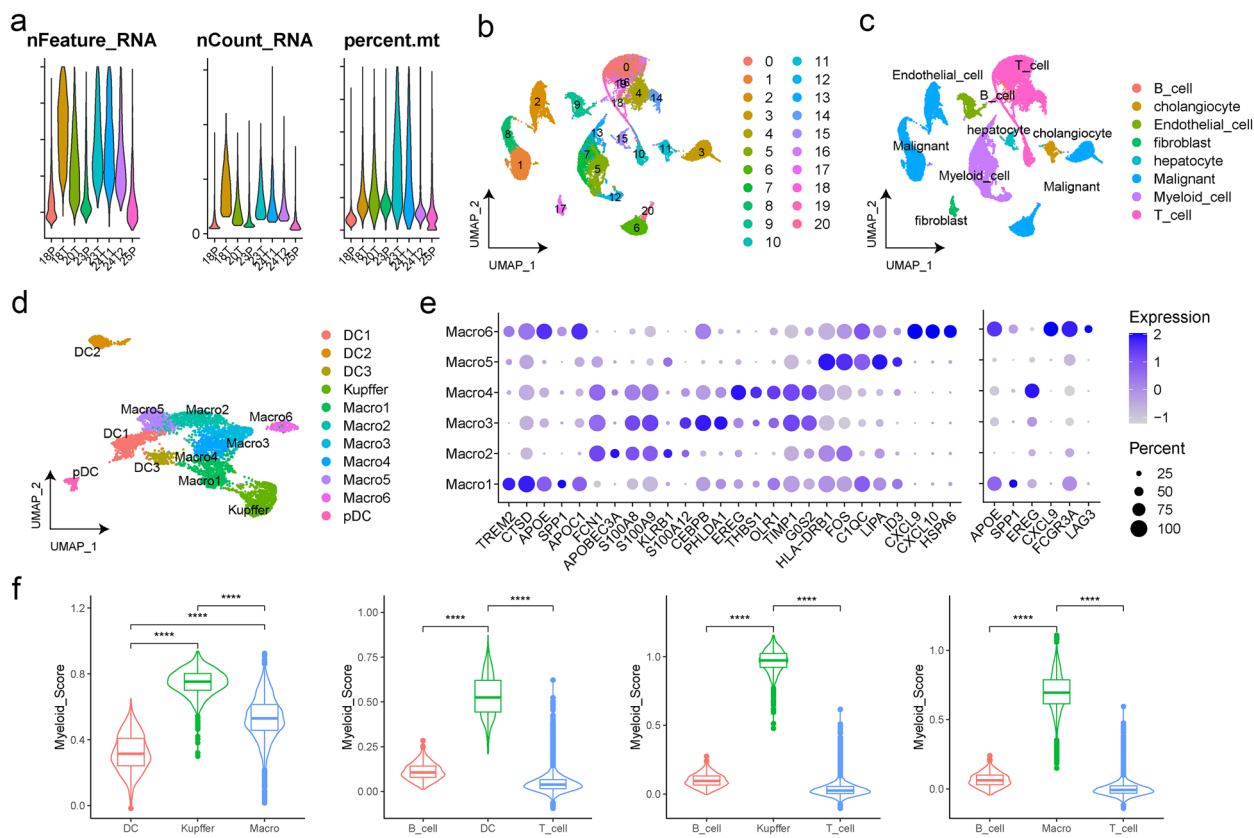
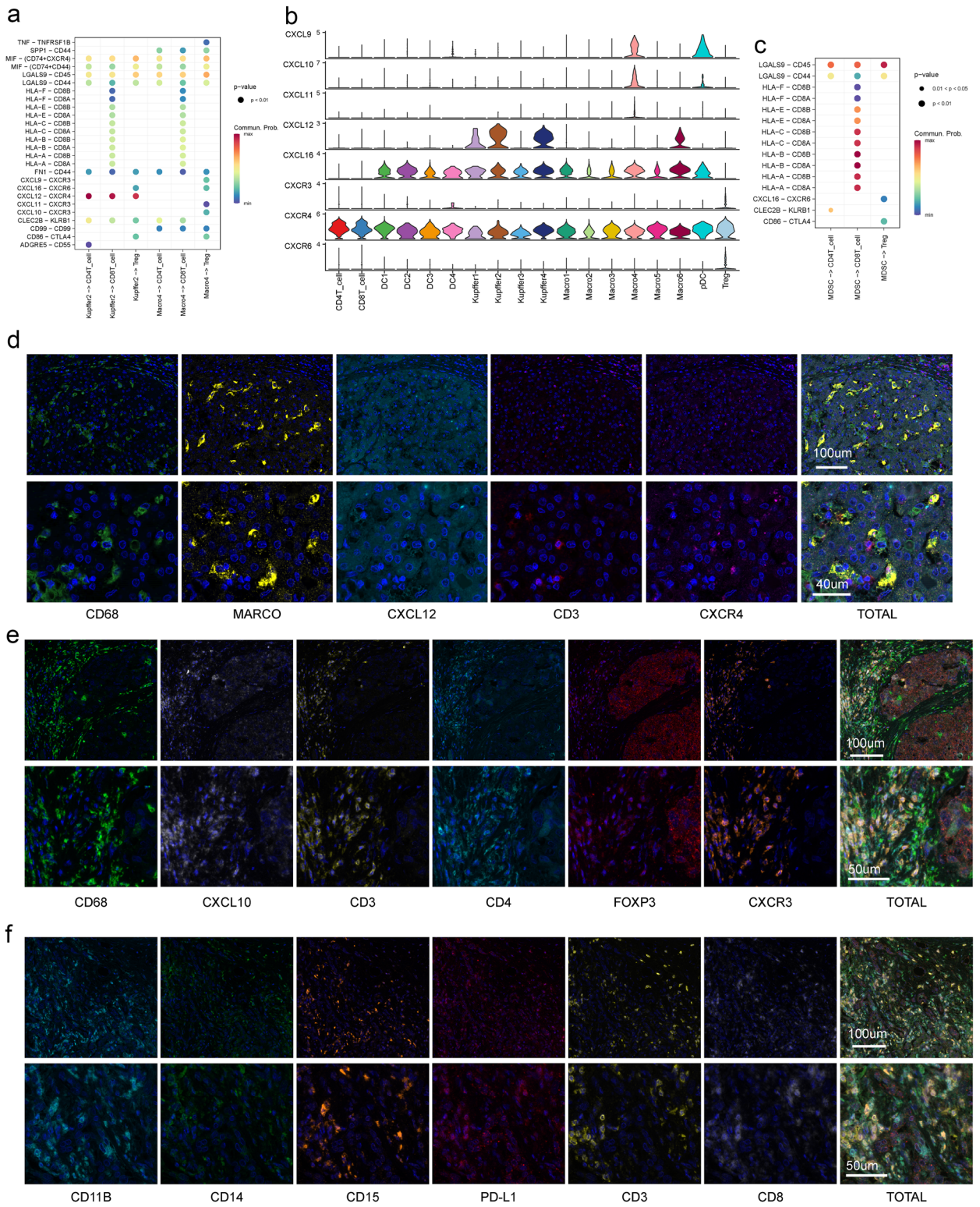


Fig. 6 Analysis and visualization for TAMs of human ICC by single-cell RNA sequencing. **a** Violin plots showed the cells expressed genes, unique molecular identifier (UMI) and mitochondrial counts for human ICC in 8 samples. **b** UMAP representation of the whole ICC as obtained from 8 human samples using dotplot. Each dot represents a single cell. **c** UMAP showed the construction of ICC atlas. **d** UMAP representation of the myeloid cells as obtained from 8 human samples using dotplot. **e** Dot plots showed the expression of top genes for ICC (left) and HCC (right) macrophages. **f** Violin plots showing the myeloid scores among myeloid cell groups and other immune cells (**** means $p < 0.0001$).



◀**Fig. 7** Intercellular communication among TAMs and T cells. **a** Dotplots showing the interactions among CXCL10+macrophages, MT1G+Kupffer cells and T cells. **b** Violin plots showing the expression of chemokines and cytokines among TAMs and T cells. **c** Dotplots showing the interactions among MDSCs and T cells. **d** mIHC of MT1G+Kupffer cells-T cells (CD68, MARCO, CXCL12, CD3, CXCR4), CXCL10+macrophages-Tregs (CD68, CXCL10, CD3, CD4, FOXP3 and CXCR3) and MDSCs-CD8+T cells (CD11B, CD14, CD15, PD-L1, CD3 and CD8) in HCC tumor tissues.

these intricate cellular communications, we conducted an intercellular analysis between TAMs (including M1, M2, MDSCs, and Kupffer cells) and other cell types. This approach enabled us to validate known mechanisms and identify potential new signaling pathways (Table S7, Fig. S5A, B). Notably, MARCO + Kupffer cells (Kupffer_1), MARCO- Kupffer cells (Kupffer_2), and pro-tumorigenic macrophages (M2) demonstrated the highest capacities for input/output interactions, indicating their active roles in TAMs communication (Fig. S6A, B).

In the identified cellular signaling pathways, TAMs primarily served as ligands (Figs. S5A and S6C). Both MARCO-Kupffer and MARCO + Kupffer cells were particularly active in this aspect (Fig. S6B). They expressed ECM-receptors, including vitronectin (VTN), and interacted with ITGAV + ITGB1 in fibroblasts and fibronectin 1 (FN1), influenced by SDC1 and SDC4 in hepatocytes. Moreover, Kupffer cells secreted cytokine and chemokine ligands (CXCL12 and CXCL16), especially in the MARCO + subgroup. These ligands interacted with C-X-C motif chemokine receptors (CXCR4 and CXCR6) in lymphocytes (CD4T, CD8T, Treg, B, plasma cells) and NK cells, playing a pivotal role in tumor progression [46]. Furthermore, both MARCO- Kupffer and M2 macrophages secreted macrophage migration inhibitory factors (MIF), targeting CD74 + CXCR4 and CD74 + CD44 in lymphocytic cells [47]. M2 macrophages also exhibited strong MIF signals, while M1 and MDSCs were considerably less active in this regard. Additionally, MARCO-Kupffer and M2 macrophages expressed secreted phosphoprotein 1 (SPP1), primarily activating CD44 in CD4 + T, Treg, and mast cells. All monocyte-derived macrophages (M1, M2, and MDSC) expressed Nicotinamide phosphoribosyltransferase (NAMPT), targeting INSR in endothelial cells, potentially mediating the NAD salvage pathway and thereby regulating the energy homeostasis of HCC [48].

In examining the effects of TAMs signaling patterns (Fig. S6D), it was found that stromal (endothelial cells and fibroblasts) and epithelial (hepatocytes) cells express MIF, which targets all TAMs (CD74 + CXCR4,

CD74 + CD44). Endothelial cells showed a particular responsiveness to amyloid precursor protein (APP), a cell membrane protein, and interacted with CD74 in TAMs. This interaction has been implicated in inhibiting Abeta production [49], thereby influencing tumor growth and metastasis [50]. Lastly, communication was observed between TAMs and various histocompatibility complex class I (HLA-A, HLA-B, HLA-C, HLA-E) and class II (HLA-DPA1, HLA-DMA, HLA-DRA) molecules expressed in lymphocytes, stromal, and epithelial cells.

TAMs Communicate with T Cells via Distinct Signaling Pathways in Hepatocellular Carcinoma

In our detailed analysis, we identified a significant abundance of MT1G + Kupffer cells within tumor tissues, which demonstrated pronounced chemotactic activity. The most prominent cellular communication pathway uncovered was the CXCL12-CXCR4 axis. This pathway was particularly notable in facilitating interactions between MT1G + Kupffer cells and T cells, as evidenced in Fig. 7a. Further gene expression analysis reinforced this observation, revealing high levels of CXCL12 expression in MT1G + Kupffer cells (Fig. 7b).

Similarly, our exploration into the role of CXCL10 + macrophages within HCC highlighted their substantial presence in tumor tissues. These macrophages actively secreted a diverse array of chemokines and cytokines, including CXCL1, CXCL9, CXCL10, and CXCL11, underscoring their pivotal role in HCC, especially in mediating communication with T cells. Notably, we discovered a unique signaling pathway facilitating communication between CXCL10 + macrophages and Tregs via the CXCL10/CXCL11-CXCR3 axis, distinct from interactions with other T cell subsets (Fig. 7a).

Gene expression profiles indicated elevated levels of CXCL9, CXCL10, and CXCL11 in CXCL10 + macrophages, while Treg cells predominantly expressed CXCR3 and CXCR6, highlighting a specialized communication route (Fig. 7b). Additionally, our observations revealed a predominant localization of MDSCs in the vicinity of tumor tissues (Fig. 4b), with significant interactions between MDSCs and T cells, particularly CD8 + T cells, through specialized pathways, including LGALS9-CD45/CD44 and HLA-A-CD8A/CD8B (Fig. 7c).

To biologically validate these intricate interactions, we utilized the multi-immunohistochemistry (mIHC) technique on HCC samples (n = 3), confirming the spatial distribution and intercellular communication

between Kupffer cells and T cells, CXCL10 + macrophages and Tregs, and MDSCs and CD8 + T cells (Fig. 7d and Fig. S7).

DISCUSSION

In this report, we present a comprehensive reference atlas of TAMs at the single cell level, derived from 17,932 TAMs within 70 human HCC samples. The identified gene expression patterns, termed Panmyeloid markers, were detected across all cohorts and most samples, significantly expanding the list of potential gene markers for myeloid cells. Specifically, we examined the cellular patterns of monocyte-derived macrophages and Kupffer cells in HCC, with a focus on their tissue locations. This work delineated the function and characteristics of two previously indistinguishable TAM populations in tumor tissues: CXCL10 + macrophages and MT1G + Kupffer cells, and explored the role of various TAM subsets within the complex cellular signaling networks among other immune cells. Notably, our findings indicate that CXCL10 + macrophages induce a transition via the CXCL10/CXCL11-CXCR3 signaling network.

A critical contribution of this study is the comprehensive characterization of single cell patterns of TAMs in HCC across three levels (Fig. 6b). To our knowledge, these levels have not been previously described and consist of: 1) the identification of 284 Panmyeloid markers, 2) a detailed description of six clusters for monocyte-derived macrophages (Macro1-Macro6) and four for Kupffer cells (Kupffer1-Kupffer4), and 3) the identification of two TAM clusters (CXCL10 + macrophages and MT1G + Kupffer cells), demonstrating significant cellular communications with T cells. Panmyeloid markers are typically associated with specific TAM functions or, in particular, with monocyte-derived macrophages and Kupffer cells. These markers are involved not only in myeloid cell migration, differentiation, cytokine production, and homeostasis, but also in pro-inflammatory or pro-tumorigenic activities. The functions of other genes from Panmyeloid markers are currently not well understood, but future investigations in this area are expected to significantly enhance our understanding of TAM biology in HCC.

Construction of the single-cell landscape of liver cirrhosis unveiled distinct populations of macrophages, notably MARCO + and TIMD4 + Kupffer cells, as well as TREM2 + CD9 + macrophages. These cells are

characterized by high expression of key pro-fibrogenic markers including IL1B, SPP1, LGALS3, CCR2, and TNFSF12. Notably, these populations expand during liver fibrosis, originate from circulating monocytes, and exhibit pro-fibrogenic properties [51]. Further investigation revealed that TREM2 + macrophages play a critical role in HCC by suppressing CD8 + T cell infiltration, primarily through the secretion of Galectin-1 [52]. Our findings also highlighted the significant expression of TREM2 in APOE + Macrol cells, suggesting a potential mechanism for T cell communication (Fig. 4, Figs. S5 and S6). Additionally, SPP1, also known as osteopontin, has been identified as a crucial marker of TAMs in HCC [53, 54]. SPP1 + macrophages, in particular, are predominantly found in AFP-positive HCC, with their receptor, CD44, present on both T cells and tumor cells [55]. The interaction between SPP1 + macrophages and fibroblasts is instrumental in forming a tumor immune barrier, which has significant implications for the efficacy of immunotherapy [56]. Furthermore, within the spectrum of pan-myeloid markers, SPP1 emerged as a top marker, notably upregulated. Macro2 cells, in particular, showed high levels of SPP1 expression. This expression plays a pivotal role in the EMT pathway and facilitates communication via the extracellular matrix receptor, underscoring its critical function in the disease pathology (Fig. 4, Table S5). Our integrated analysis revealed the existence of two novel TAM subpopulations in HCC tumors and adjacent tissues, characterized by relatively high levels of CXCL10 + macrophages and MT1G + Kupffer cells. These findings suggest their potential roles in the occurrence and development of HCC, notably effects initially described at the single cell level. Studies such as Yuan et al. [57] have demonstrated that activated CD4 + T cells in HCCs stimulate CXCL10 production by macrophages, which then binds CXCR3 on B cells, enabling their transformation to IgG-producing plasma cells. This IgG production activates Fc receptors in macrophages to produce cytokines, reducing anti-tumor immune responses. Similarly, Liu et al. [58] reported that selective recruitment of CXCR3 + B cells bridges pro-inflammatory interleukin-17 responses with pro-tumorigenic macrophage polarization in the tumor milieu. Our current data expand the understanding of macrophage functions by demonstrating that CXCL10 + macrophages communicate with CXCR3 + Treg cells to induce downstream signaling pathways. The presence of CXCL12-CXCR4 signaling

Integrated single cell analysis reveals an atlas of tumor associated...

pathways within cells in HCC has also been noted in several studies, such as the one by Chen et al. [59], suggesting that these factors may be targets for inhibiting crosstalk among tumor cells, cancer-associated fibroblasts (CAFs), and TAMs. Our findings provide the first evidence indicating that MT1G + Kupffer cells communicate with T cells to inhibit tumor progression in HCC. MT1G, significantly downregulated in tumor tissues, is known to inhibit proliferation and enhance apoptosis of HCC cells [43]. Our data suggest that MT1G in Kupffer cells within tumor tissues may involve a mechanism that increases the stability of p53 by inhibiting MDM2 expression, broadening our understanding of tumor suppression factors.

However, our study has limitations. First, the construction of a comprehensive atlas of myeloid cells required a data integration technique, potentially introducing batch effects due to sample processing, library preparation, and sequencing. Despite efforts to minimize these effects, a potential bias remains, prompting the use of algorithms to reduce this influence. Moreover, part of samples was unknown viral status and tumor stage, and the TAM populations could be influenced by aetiology and stage of liver disease. And if HCC samples were obtained from cirrhotic patients were unknown. Second, while we validated the existence of CXCL10 + macrophages and MT1G + Kupffer cells at the single cell level, additional assays such as immunohistochemistry and immunofluorescence, as well as spatial transcriptomes, were not included. Third, although our analyses of cellular communications indicate potential signaling pathways using specific marker gene expressions, functional experiments are necessary to substantiate the exact pathways involved.

CONCLUSIONS

The establishment of transcriptomic profiles and the elucidation of cellular communications within the intricate microenvironment of human HCC are pivotal in understanding the underlying molecular mechanisms of this disease. Our comprehensive myeloid cell atlas serves as a foundational contribution to the field of HCC research. This atlas not only advances our understanding of the disease's molecular landscape but also sheds light on the critical role of TAMs in HCC. The insights gained from this study underscore the importance of cellular interactions and gene expression patterns in deciphering

the complex dynamics of the HCC microenvironment. Our findings pave the way for future research and potential therapeutic interventions targeting TAMs, offering new avenues to combat this challenging malignancy.

METHODS

Data Preparation

We identified 4 public scRNA-seq human HCC datasets using the 10X chromium single cell RNA seq platform. Processed data were downloaded from the Gene Expression Omnibus (GEO) repository (<https://www.ncbi.nlm.nih.gov/geo/>), and included GSE140228 [10], GSE125449 [12], GSE149614 [60] and GSE156625 [8]. We restricted the datasets including technique (10X Genomics), disease (HCC) and species (human). The stages of patients were classified according to the guidance of AJCC version 8. And we used integration function to remove batch effect. Detailed information on these procedures is contained in Table S1. For the bulk RNA-seq data, we downloaded TCGA Liver Cancer (LIHC, N = 423) from the UCSC Xena database (<https://xenabrowser.net/datapages/>), which included gene expressions and survival phenotypes. A downstream analysis was then performed on these data. To discuss whether the finding of HCC is unique, we acquired a public scRNA-seq human intrahepatic cholangiocarcinoma (ICC) cohort dataset (GSE138709) using the 10X chromium single cell RNA seq platform.

Preprocessing and Integration of scRNA-seq Data

The Seurat R package (version 3.2.0) [13], a tool for single cell genomics, was used to process the single cell RNA sequencing data. Identical exclusion criteria were employed for the 4 datasets and included cells with < 501 expressed genes or > 25% mitochondrial counts. Based on this criteria, 135,900 high quality cells were used for downstream analysis.

For data integration, we used Seurat's functions, including FindIntegrationAnchors and IntegrateData to merge the datasets. Details regarding this technique are contained in the website (https://satijalab.org/seurat/articles/integration_introduction.html). Cells were normalized and scaled with the default parameters and their highly variable features were determined using FindVariableFeatures function. PCA analysis was then performed with the variable features that had

been identified. Dimension reduction and clustering were conducted using FindNeighbors (dims = 1:10) and FindClusters (resolution = 0.5) functions. Finally, a non-linear dimensional reduction (UMAP) was performed to assess and visualize the data.

Identification of Differentially Expressed Genes

FindMarkers and FindAllMarkers functions were used to locate differentially expressed features according to clusters, cell types and tissue locations. The threshold for logFC was 0.25 while the minimum fraction of genes detected in cells was 0.1, with default.

Cell Type Annotation

Cell types were annotated to known biological types with canonical marker genes (Table S2). Within the entire atlas, cells were annotated as immune (Myeloid cells, CD4+ T cells, CD8+ T cells, regulatory T (Treg), natural killer (NK) cells, B cells and Mast cells) or non-immune (Endothelial cells, Fibroblasts and Hepatocytes) phenotypes. In addition, the SingleR package (version 1.2.4) was used to facilitate the identification of cell types.

Myeloid Score Analysis

For the gene set analysis, the 'AddModuleScore' function from the Seurat package was employed. This process entailed using particular gene sets of interest. Subsequently, a score was calculated for every cell based on the expression levels of genes in each set, facilitating a comprehensive analysis of gene expression patterns at the cellular level.

Functional Enrichment Analysis

Following the annotation of each cell type, we conducted functional enrichment analysis on genes expressed differentially across various clusters. This analysis, aimed at elucidating the biological processes and potential functions of distinct cells, was carried out utilizing the clusterProfiler package (version 4.6.2) [61] and the org.Hs.eg.db package (version 3.16.0) for Gene Ontology (GO) and KEGG (Kyoto Encyclopedia of Genes and Genomes) analysis. The threshold for significance in both GO and KEGG analyses was set at a p-value of 0.05. The top terms were presented through either barplots or

dotplots, providing a visual representation of the functional enrichment.

Survival Analysis

A survival analysis was conducted from the survival data of TCGA LIHC. The survival (version 3.2.3) and survminer (version 0.4.8) R package with default parameters was used to assess levels of gene expression.

Copy Number Variation Analysis

To deduce copy number variations (CNVs) from scRNA-seq data, a method detailed in a previous publication [62] was utilized. The procedure was conducted employing the R code found at <https://github.com/broadinstitute/inferCNV>, with the application of default settings. The approach began with the identification of likely nonmalignant cells, which included manually annotated immune cells (T cells, B cells, and myeloid cells) and stromal cells (endothelial cells and fibroblasts). The CNV estimates obtained from these cells served as the baseline for analysis. Reference groups were then adjusted based on the preliminary inferCNV outcomes. These adjustments informed further analysis rounds, facilitating a more precise and detailed CNV evaluation.

Cellular Communication Analysis

Cell to cell interactions were evaluated using the latest version of the CellChat package (version (1.1.2)) [63]. Three major signaling pathways were included: secreted signaling, extracellular matrix (ECM)-receptor and cellular contact. The majority of ligand-receptor interactions were mainly based on the Kyoto Encyclopedia of Genes and Genomes (KEGG) signaling pathway database and recent peer-reviewed experimental studies. The main steps for assessing intercellular communication consisted of: 1) Identification of differentially expressed signaling genes 2) Calculations of average ensemble expressions and 3) Calculations of intercellular communication probability.

Immunohistochemical Staining Analysis

Paraffin sections are routinely dewaxed to hydration, and washed with distilled water. Following incubation in 3% H₂O₂ for 10 min, antibodies anti- CD14, CD68, CD4

Integrated single cell analysis reveals an atlas of tumor associated...

and CD8 were added and incubated at 4 °C for overnight. The specimens were incubated with secondary antibodies at 37°C for 1 h, followed by diaminobenzidine staining [64]. All samples were collected from patients who underwent liver transplantation, which were approved by the Ethics Committee of the Affiliated Hospital of Qingdao University.

Multiplex Immunofluorescence Staining

Briefly, slides were rehydrated with a series of graded ethanol solutions in deionized water. Antigen retrieval was performed, then slides were serially stained with the following antibodies: CD14, CD11b, PD-L1 and CD8. Subsequently, Opal IHC Detection Kit (Akoya Biosciences) was applied as a secondary label and antibody signals. Image acquisitions were performed using the Vectra Polaris multispectral imaging platform (Akoya Biosciences), with the entire slide image being scanned and 3–5 representative regions of interest chosen by the pathologist [65].

Statistical Analysis

We used Student's t-test to compare gene expression level between tumor tissues and normal tissues. Kaplan–Meier analysis with the log-rank test was performed to evaluate the OS of each group. All statistical analyses were performed using R software (version 4.0.2) and its appropriate packages. P-values < 0.05 was considered statistically significant.

SUPPLEMENTARY INFORMATION

The online version contains supplementary material available at <https://doi.org/10.1007/s10753-024-02026-1>.

ACKNOWLEDGEMENTS

The authors would like to thank the Organ Transplantation Center and the Key Laboratory of Organ Transplantation of Affiliated Hospital of Qingdao University for their technical support. We thank Pro. Tao Shan (Medical College of Qingdao University) and all the members of his anatomy research team for support. We also thank Dr. Jianming Zeng (University of Macau), and all the members of his bioinformatics team, biotrainee, for generously sharing their experience and codes.

AUTHORS' CONTRIBUTIONS

Jinzheng Cai, Shipeng Li and Xinqiang Li contributed to the research design. Xinqiang Li, Ruixia Li, Xiaolong Miao, Bin Wu

and Chengyu Wang contributed to the data management and statistical analyses. Jinzheng Cai, Ruixia Li, Xinqiang Li, Xin Zhou and Junjing Cao wrote the manuscript. All authors reviewed the manuscript. Xinqiang Li and Ruixia Li contributed equally to this work.

FUNDING

This work was supported by the National Natural Science Foundation of China (No. 82370666), the Science Foundation of Shandong Province (No. ZR2022MH292), the Science Foundation of the Fujian Province, China (No. 2021J01779 and No. 2021J02041), Joint Funds for the Innovation of Science and Technology, Fujian Province (No. 2020Y9089), and Science Foundation of Fujian Medical University Union Hospital (No. 2020XH009 and 2020XH012).

AVAILABILITY OF DATA AND MATERIALS

All data generated or analyzed during this study are available in this article.

DECLARATIONS

Ethics approval and consent to participate The study protocol was approved by the ethics committee of Affiliated Hospital of Qingdao University. All subjects provided informed consent and all experiments were conducted per the study protocol.

Consent for publication All authors have reviewed the manuscript and have given consent for publication.

Competing interests The authors declare no conflicts of interest in this work.

REFERENCES

1. Chidambaramathan-Reghupaty, S., P.B. Fisher, and D. Sarkar. 2021. Hepatocellular carcinoma (HCC): Epidemiology, etiology and molecular classification. *Advances in Cancer Research* 149: 1–61.
2. Zhao, J., et al. 2020. Single-cell RNA sequencing reveals the heterogeneity of liver-resident immune cells in human. *Cell Discovery* 6: 22.
3. Dou, L., et al. 2019. Macrophage Phenotype and Function in Liver Disorder. *Frontiers in Immunology* 10: 3112.
4. Wen, Y., et al. 2021. Hepatic macrophages in liver homeostasis and diseases-diversity, plasticity and therapeutic opportunities. *Cellular & Molecular Immunology* 18 (1): 45–56.
5. Cheng, K., et al. 2022. Tumor-associated macrophages in liver cancer: From mechanisms to therapy. *Cancer Communications (Lond)* 42 (11): 1112–1140.
6. Mo, Z., et al. 2022. Single-cell transcriptomics reveals the role of Macrophage-Naive CD4 + T cell interaction in the

- immunosuppressive microenvironment of primary liver carcinoma. *Journal of Translational Medicine* 20 (1): 466.
7. Sun, Y., et al. 2021. Single-cell landscape of the ecosystem in early-relapse hepatocellular carcinoma. *Cell* 184 (2): 404–442.
 8. Sharma, A., et al. 2020. Onco-fetal Reprogramming of Endothelial Cells Drives Immunosuppressive Macrophages in Hepatocellular Carcinoma. *Cell* 183 (2): 377–394.
 9. MacParland, S.A., et al. 2018. Single cell RNA sequencing of human liver reveals distinct intrahepatic macrophage populations. *Nature Communications* 9 (1): 4383.
 10. Zhang, Q., et al. 2019. Landscape and Dynamics of Single Immune Cells in Hepatocellular Carcinoma. *Cell* 179 (4): 829–845.
 11. Zheng, C., et al. 2017. Landscape of Infiltrating T Cells in Liver Cancer Revealed by Single-Cell Sequencing. *Cell* 169 (7): 1342–1356.
 12. Ma, L., et al. 2019. Tumor Cell Biodiversity Drives Microenvironmental Reprogramming in Liver Cancer. *Cancer Cell* 36 (4): 418–430.
 13. Stuart, T., et al. 2019. Comprehensive Integration of Single-Cell Data. *Cell* 177 (7): 1888–1902.
 14. Qiu, Y., et al. 2021. Next frontier in tumor immunotherapy: Macrophage-mediated immune evasion. *Biomark Research* 9 (1): 72.
 15. Lu, C., et al. 2019. Current perspectives on the immunosuppressive tumor microenvironment in hepatocellular carcinoma: Challenges and opportunities. *Molecular Cancer* 18 (1): 130.
 16. Rafalik, M., et al. 2019. The identification of discontinuous epitope in the human cystatin C - Monoclonal antibody HCC3 complex. *Journal of Proteomics* 191: 58–67.
 17. Yang, F., et al. 2020. Interaction with CD68 and Regulation of GAS6 Expression by Endosialin in Fibroblasts Drives Recruitment and Polarization of Macrophages in Hepatocellular Carcinoma. *Cancer Research* 80 (18): 3892–3905.
 18. De Ponti, A., et al. 2015. A pro-tumorigenic function of S100A8/A9 in carcinogen-induced hepatocellular carcinoma. *Cancer Letters* 369 (2): 396–404.
 19. Fan, J., et al. 2021. Expression of leukocyte immunoglobulin-like receptor subfamily B expression on immune cells in hepatocellular carcinoma. *Molecular Immunology* 136: 82–97.
 20. Qian, B.Z., and J.W. Pollard. 2010. Macrophage diversity enhances tumor progression and metastasis. *Cell* 141 (1): 39–51.
 21. Sica, A., P. Invernizzi, and A. Mantovani. 2014. Macrophage plasticity and polarization in liver homeostasis and pathology. *Hepatology* 59 (5): 2034–2042.
 22. Liang, Y., et al. 2019. Thymic stromal lymphopoietin epigenetically upregulates Fc receptor gamma subunit-related receptors on antigen-presenting cells and induces T(H)2/T(H)17 polarization through dectin-2. *The Journal of Allergy and Clinical Immunology* 144 (4): 1025–1035.
 23. Liu, H., et al. 2013. Characterization of fibrinogen-like protein 2 (FGL2): Monomeric FGL2 has enhanced immunosuppressive activity in comparison to oligomeric FGL2. *International Journal of Biochemistry & Cell Biology* 45 (2): 408–418.
 24. Bchir, S., et al. 2021. Impact of cathepsin D activity and C224T polymorphism (rs17571) on chronic obstructive pulmonary disease: Correlations with oxidative and inflammatory markers. *Clinical and Experimental Medicine* 21 (3): 457–465.
 25. Chen, J., J.A. Gingold, and X. Su. 2019. Immunomodulatory TGF-beta Signaling in Hepatocellular Carcinoma. *Trends in Molecular Medicine* 25 (11): 1010–1023.
 26. Morse, M.A., et al. 2019. The Role of Angiogenesis in Hepatocellular Carcinoma. *Clinical Cancer Research* 25 (3): 912–920.
 27. Kumar, A.R., et al. 2021. Anti-VEGF Mediated Immunomodulatory Role of Phytochemicals: Scientific Exposition for Plausible HCC Treatment. *Current Drug Targets* 22 (11): 1288–1316.
 28. Xiao, Z., Y. Wang, and H. Ding. 2019. XPD suppresses cell proliferation and migration via miR-29a-3p-Mdm2/PDGF-B axis in HCC. *Cell & Bioscience* 9: 6.
 29. Liu, Y., et al. 2019. CKLF1 Enhances Inflammation-Mediated Carcinogenesis and Prevents Doxorubicin-Induced Apoptosis via IL6/STAT3 Signaling in HCC. *Clinical Cancer Research* 25 (13): 4141–4154.
 30. Li, J., et al. 2020. The novel interplay between CD44 standard isoform and the caspase-1/IL1B pathway to induce hepatocellular carcinoma progression. *Cell Death & Disease* 11 (11): 961.
 31. Wang, D., et al. 2019. APOBEC3B interaction with PRC2 modulates microenvironment to promote HCC progression. *Gut* 68 (10): 1846–1857.
 32. Peng, Z.P., et al. 2020. Glycolytic activation of monocytes regulates the accumulation and function of neutrophils in human hepatocellular carcinoma. *Journal of Hepatology* 73 (4): 906–917.
 33. Tian, X., et al. 2019. Tumor-derived exosomes, myeloid-derived suppressor cells, and tumor microenvironment. *Journal of Hematology & Oncology* 12 (1): 84.
 34. Wei, T., et al. 2020. The Significance of Secreted Phosphoprotein 1 in Multiple Human Cancers. *Frontiers in Molecular Biosciences* 7: 565383.
 35. House, I.G., et al. 2020. Macrophage-Derived CXCL9 and CXCL10 Are Required for Antitumor Immune Responses Following Immune Checkpoint Blockade. *Clinical Cancer Research* 26 (2): 487–504.
 36. Rahma, O.E., and F.S. Hodi. 2019. The Intersection between Tumor Angiogenesis and Immune Suppression. *Clinical Cancer Research* 25 (18): 5449–5457.
 37. Nemeth, J., et al. 2009. S100A8 and S100A9 are novel nuclear factor kappa B target genes during malignant progression of murine and human liver carcinogenesis. *Hepatology* 50 (4): 1251–1262.
 38. Wilson, C.L., et al. 2015. NFkappaB1 is a suppressor of neutrophil-driven hepatocellular carcinoma. *Nature Communications* 6: 6818.
 39. Cheng, W.L., et al. 2021. The Role of EREG/EGFR Pathway in Tumor Progression. *International Journal of Molecular Sciences* 22(23).
 40. Tacke, F. 2017. Targeting hepatic macrophages to treat liver diseases. *Journal of Hepatology* 66 (6): 1300–1312.
 41. Blauw, L.L., et al. 2020. A Novel Role for CETP as Immunological Gatekeeper: Raising HDL to Cure Sepsis? *Trends in Endocrinology and Metabolism* 31 (5): 334–343.
 42. Wang, Y., et al. 2015. Plasma cholesteryl ester transfer protein is predominantly derived from Kupffer cells. *Hepatology* 62 (6): 1710–1722.
 43. Wang, Y., et al. 2019. MT1G serves as a tumor suppressor in hepatocellular carcinoma by interacting with p53. *Oncogenesis* 8 (12): 67.
 44. Li, C., et al. 2014. AEG-1 Promotes Metastasis Through Downstream AKR1C2 and NF1 in Liver Cancer. *Oncology Research* 22 (4): 203–211.
 45. Li, C., et al. 2016. High-Content Functional Screening of AEG-1 and AKR1C2 for the Promotion of Metastasis in Liver Cancer. *Journal of Biomolecular Screening* 21 (1): 101–107.
 46. Yang, J., et al. 2019. TCF12 promotes the tumorigenesis and metastasis of hepatocellular carcinoma via upregulation of CXCR4 expression. *Theranostics* 9 (20): 5810–5827.
 47. Hughes, C.E., and R.J.B. Nibbs. 2018. A guide to chemokines and their receptors. *FEBS Journal* 285 (16): 2944–2971.

48. Schuster, S., et al. 2015. FK866-induced NAMPT inhibition activates AMPK and downregulates mTOR signaling in hepatocarcinoma cells. *Biochemical and Biophysical Research Communications* 458 (2): 334–340.
49. Matsuda, S., Y. Matsuda, and L. D'Adamio. 2009. CD74 interacts with APP and suppresses the production of Abeta. *Molecular Neurodegeneration* 4: 41.
50. Wu, X.L., et al. 2020. Amyloid precursor protein regulates 5-fluorouracil resistance in human hepatocellular carcinoma cells by inhibiting the mitochondrial apoptotic pathway. *Journal of Zhejiang University. Science. B* 21 (3): 234–245.
51. Ramachandran, P., et al. 2019. Resolving the fibrotic niche of human liver cirrhosis at single-cell level. *Nature* 575 (7783): 512–518.
52. Tan, J., et al. 2023. TREM2(+) macrophages suppress CD8(+) T-cell infiltration after transarterial chemoembolisation in hepatocellular carcinoma. *Journal of Hepatology* 79 (1): 126–140.
53. Cheng, S., et al. 2021. A pan-cancer single-cell transcriptional atlas of tumor infiltrating myeloid cells. *Cell* 184 (3): 792–809.
54. Wei, J., et al. 2021. Characterizing Intercellular Communication of Pan-Cancer Reveals SPP1+ Tumor-Associated Macrophage Expanded in Hypoxia and Promoting Cancer Malignancy Through Single-Cell RNA-Seq Data. *Frontiers in Cell and Development Biology* 9: 749210.
55. He, H., et al. 2023. Multi-dimensional single-cell characterization revealed suppressive immune microenvironment in AFP-positive hepatocellular carcinoma. *Cell Discovery* 9 (1): 60.
56. Liu, Y., et al. 2023. Identification of a tumour immune barrier in the HCC microenvironment that determines the efficacy of immunotherapy. *Journal of Hepatology* 78 (4): 770–782.
57. Wei, Y., et al. 2019. Plasma Cell Polarization to the Immunoglobulin G Phenotype in Hepatocellular Carcinomas Involves Epigenetic Alterations and Promotes Hepatoma Progression in Mice. *Gastroenterology* 156 (6): 1890–1904.
58. Liu, R.X., et al. 2015. Chemokine (C-X-C motif) receptor 3-positive B cells link interleukin-17 inflammation to protumorigenic macrophage polarization in human hepatocellular carcinoma. *Hepatology* 62 (6): 1779–1790.
59. Chen, S., et al. 2021. Cancer-associated fibroblast-induced M2-polarized macrophages promote hepatocellular carcinoma progression via the plasminogen activator inhibitor-1 pathway. *International Journal of Oncology* 59(2).
60. Lu, Y., et al. 2022. A single-cell atlas of the multicellular ecosystem of primary and metastatic hepatocellular carcinoma. *Nature Communications* 13 (1): 4594.
61. Wu, T., et al. 2021. ClusterProfiler 4.0: A universal enrichment tool for interpreting omics data. *Innovation (Camb)* 2 (3):100141.
62. Venteicher, A.S., et al. 2017. Decoupling genetics, lineages, and microenvironment in IDH-mutant gliomas by single-cell RNA-seq. *Science* 355(6332).
63. Jin, S., et al. 2021. Inference and analysis of cell-cell communication using Cell Chat. *Nature Communications* 12 (1): 1088.
64. Li, S., et al. 2021. Autophagic activation of IRF-1 aggravates hepatic ischemia-reperfusion injury via JNK signaling. *MedComm* 2020 2 (1): 91–100.
65. Li, S.P., et al. 2022. Multiplex Immunofluorescence for Detection of Spatial Distributions of Infiltrating T Cells Within Different Regions of Hepatic Lobules During Liver Transplantation Rejection. *Inflammation* 45 (2): 651–664.

Publisher's Note Springer Nature remains neutral with regard to jurisdictional claims in published maps and institutional affiliations.

Springer Nature or its licensor (e.g. a society or other partner) holds exclusive rights to this article under a publishing agreement with the author(s) or other rightsholder(s); author self-archiving of the accepted manuscript version of this article is solely governed by the terms of such publishing agreement and applicable law.